Progress In Electromagnetics Research M, Vol. 116, 165–176, 2023

Hyperbolic Graded Index Biophotonic Cholesterol Sensor with Improved Sensitivity

Diptimayee Dash and Jasmine Saini*

Abstract—A novel approach is presented to achieve improved sensing performance using a one-dimensional (1D) hyperbolic graded photonic crystal (PC). The graded structure achieves refractive index modulation that varies hyperbolically with layer depth, due to its graded index geometry. Porous materials are employed to facilitate analyte infiltration. The reflectivity and sensing performance of the proposed graded and non-graded geometry is evaluated using the transfer matrix method (TMM). The sensing capability of the graded structure is evaluated analytically by infusing different analytes within the cavity, considering various cavity widths and incidence angles. At a 40-degree angle of incidence, the analytical results demonstrate that the suggested graded structure exhibits a maximum sensitivity of 469 nm/RIU, along with a detection limit and FOM of 9.1×10^{-3} and 125 RIU^{-1}, respectively. The detailed electric field confinement of the graded geometry is also carried out at the interface. The proposed structure outperforms conventional non-graded structures with a 114% higher sensitivity. The bio-photonic design can be easily implemented and provides high performance compared to previous works that employ exponentially graded structures. The suggested biosensor can detect even minor fluctuations in the refractive index of blood serum samples with different cholesterol concentrations.

1. INTRODUCTION

Recently, researchers globally are focusing on the evolution of biosensors with fast response time and low-level label-free detection capability. Although the standard analytical methods provide a high level of accuracy, they are very costly and need lots of analytes for detection purposes. Photonic crystals (PCs), which refer to periodic multilayer refractive index structures, have recently become popular due to their exceptional performance, easy structural analysis, cost-effectiveness, and simple fabrication process [1, 2]. In recent years, the demand for resonating one-dimensional (1D) PC devices has significantly increased in a variety of electric field confinement [3, 4], including liquid sensing, gas sensing [5], and biosensing [6]. PC sensors typically assess various optical characteristics like transmittance spectrum, reflectivity, photonic bandgap, and surface electric field confinement to detect changes in the refractive index of analytes. Conventional non-graded PCs are constructed using periodic layers of one or two materials of different refractive indices. The localization of the defect mode within the photonic bandgap (PBG) is affected by the dimension and refractive index of the cavity layer that has a consistent periodicity. Adjusting the width of the cavity layer and incidence angle can improve the sensitivity of the conventional non-graded geometry.

The graded refractive index (GReI) PC is a technique that has been considered in this case [7]. Numerous studies have shown that GReI structures have refractive index profiles that gradually change along the width of the layers [8]. GReI PCs can be constructed by altering photonic crystals' filling factor, optical index, and lattice period [9]. The refractive index changes of 1D photonic crystals can

Received 23 March 2023, Accepted 29 April 2023, Scheduled 11 May 2023

* Corresponding author: Jasmine Saini (jasmine.saini@jiit.ac.in).

The authors are with the Department of Electronics & Communication Engineering, Jaypee Institute of Information Technology, Noida, Uttar Pradesh-201309, India.

be realized by adjusting the aforementioned factors. GReI PCs differ from homogeneous materials in that they contain distinguishing characteristics. To create the appropriate refractive index contrast, GReI PCs can be utilized in place of other various dielectric refractive index materials. Compared to a traditional non-graded structure, the performance of GReI PCs offers greater design freedom. GReI PCs' incredible qualities include tunability, super lensing, enhanced light-matter interaction, and low-loss propagations.

J. Russel was the first person who studied Graded PCs and their theoretical aspects [10], and subsequently, the first graded PC structure was proposed by Centeno et al. [11, 12]. The influence of grading profile (exponential, hyperbolic, and linear) on the bandgap, phase shift, group velocity, delay time, and field distribution has been reported by Singh et al. [13]. As a result of the numerous advantages offered by GReI PCs, they have been applied in various fields, such as optical filters, sensing and detection, controlling photonic bandgaps via refractive index, photonic integrated circuits, and tuning defect modes in graded defect layers for filtering applications [14].

All animal cell membranes include cholesterol, a form of lipid that is essential to their structural strength. Hypercholesterolemia is characterized by a concentration of cholesterol exceeding the normal level of 200 mg/dl, typically above 240 mg/dl. Heart disease, atherosclerosis, hypertension, and coronary heart disease are just a few of the difficulties that high cholesterol levels cause [15]. On the other hand, hypercholesterolemia results in anaemia and hepatopathy. Therefore, it is crucial to check your cholesterol levels regularly. Numerous methods have been used to measure the level of cholesterol, including colorimetric [16], spectrophotometry [17], and high performance liquid chromatography (HPLC) [18]. Still, the 1D photonic crystal resonator-based sensor is favoured chiefly because of its real-time monitoring, miniaturization, high sensitivity, and wide range of applications.

This paper analyses a hyperbolically graded resonator (HGR) based 1D photonic structure and shows how the GReI PCs control and manipulate the light energy within it and demonstrate a significant impact. This study presents a hyperbolic variation in the refractive index to the width of the dielectric structure, which is incremental. The structure comprises a bilayer 1D PC of graded index porous silicon (refractive index (RI) varying from 1.6 to 3.45) and porous silicon (RI of 1.6) layers. The high index layer's refractive index hyperbolically varies with the layer's width. Porous material makes the easy infiltration of analytes into the structure, thereby influencing the structure's sensitivity [19, 20]. Also, it provides a high index contrast to the structure using the same material. Device performances of both the conventional non-graded and HGR structures are investigated and compared with varying incidence angles, cavity thickness, and different analyte infiltration. Finally, the HGR structure attains a 114% higher sensitivity than the conventional non-graded structure.

The paper is structured as follows. Section 2 employs the TMM matrix to showcase the concept of reflectivity in multi-layered 1D GReI PCs. The impact on bandgap, resonant frequency, and sensitivity of 1D photonic structures based on NGR and HGR is described in Section 3. Furthermore, the research investigates the effect of various defect layer thicknesses and incidence angles on the sensitivity of the suggested structure. Lastly, Section 4 outlines the conclusion of the paper.

2. PROPOSED STRUCTURAL DESIGN

In this paper, Figure 1(a) exhibits a resonator with a step-index multilayer structure (non-graded) where the refractive index changes based on the thickness of each layer. This resonator consists of two dielectric layers with an unchanging refractive index. Conversely, Figure 1(b) showcases a graded-index multilayer resonator with a hyperbolic variation in refractive index in one type of dielectric layer as a function of cavity layer thickness. The other type of dielectric layer is homogeneous and has a constant refractive index.

The refractive index range of dielectric materials typically falls between 1.6 and 3.45, which coincides with the refractive index variation of the dielectric layer having a hyperbolic graded index. The introduction of porosity could facilitate the physical implementation of the graded structure. Silicon (Si) is a dielectric substance whose refractive index (3.45) is determined using the Sellmeier approximation [19], resulting in a range of 3.45 (porosity 0%) to 1.6 (porosity 80%) as indicated [20]. To ensure appropriate infiltration of analytes, the graded layer is believed to be porous, and Equation (1)

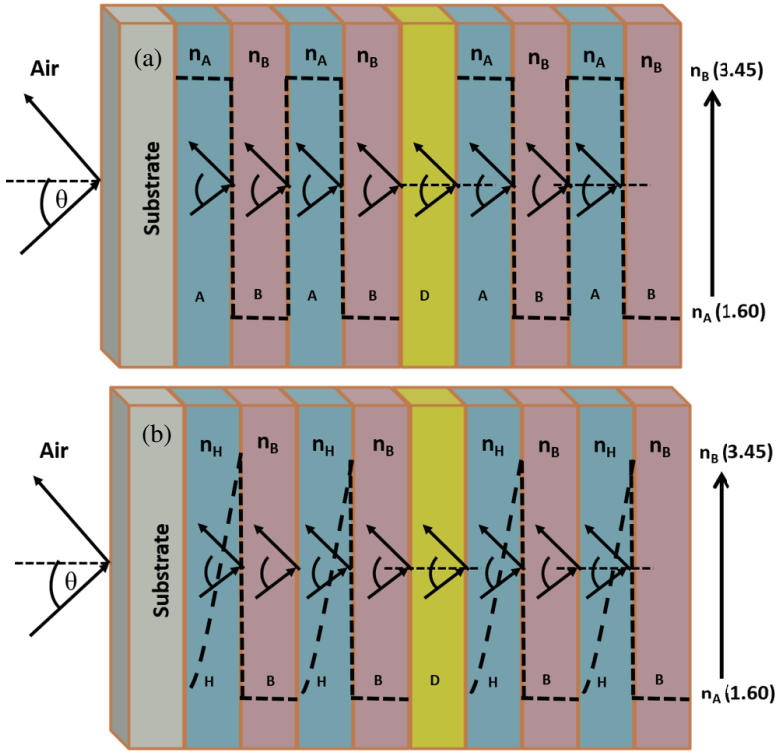

Figure 1. (a) The first structure described is a non-graded geometry with accompanied by its corresponding variation in refractive index denoted by a black dotted line. (b) The second structure is a hyperbolically graded geometry, also depicted with its corresponding variation in refractive index shown by a black dotted line.

can be employed to calculate the porosity (P) of each layer [21].

$$P = \frac{(n_{pm}^2 - n_{dm}^2)(n_{an}^2 - 2n_{dm}^2)}{(n_{pm}^2 + 2n_{dm}^2)(n_{an}^2 - n_{dm}^2)} \tag{1}$$

where n_{dm}, n_{pm}, and n_{an} are the refractive indices of dense material, porous material, and air/analytes, respectively. Modifying the porosity will have an impact on the effective refractive index of the layer, thereby affecting the transmission and reflection spectrum. Greater porosity enhances analyte infiltration and sensitivity, but it also impacts the strength of the reflected signal. But with increasing porosity, the geometry becomes more fragile. Therefore, 80% porosity is taken into consideration.

Using the distributed Bragg reflector formula by $n_j d_j = (\lambda/4)$, a non-graded multilayer resonator comprising a PC structure made of materials A (of silicon having RI (3.45)) and B (of porous silicon having RI (1.6)) is considered [22, 23]. It comprises four alternate layers ($N = 4$) of materials "A" and "B" thus forming a "$(A/B)^4/D/(A/B)^4$" configuration as shown in Figure 1(a). The geometry possesses a photonic bandgap of width 1063 nm (1320 nm–2383 nm) for considered layer thickness of D_A (112 nm) and D_B (242 nm), respectively. The defect layer "D" has a refractive index (n_{defect}) and a width of d_{defect}). Assuming a resonating wavelength of 1550 nm for the structure, the values of n_j and d_j in the distributed Bragg reflector formula correspond to the refractive index and thickness of the jth layer. A photonic crystal with a hyperbolic graded refractive index, comprising a cavity layer arranged in the form of "$(H/B)^4/D/(H/B)^4$", constitutes the hyperbolic graded index multilayer resonator. In this structure, "H" represents the hyperbolic graded refractive index material, and the refractive index distributions within the graded "H" vary hyperbolically in accordance with the width of the layer, ranging from 1.6 to 3.45, as depicted in Figure 1(b). Meanwhile, "B" denotes the layer with a low refractive index (n_l) of 1.6 (Si with 80% porosity) and a width of D_B. By taking the average of the

high and low refractive index values of the hyperbolic graded layer, denoted as n_H, the thickness of the hyperbolic graded layer can be calculated as $D_H = \lambda/(4 * n_H)$. The structure possesses a photonic bandgap of width 1066 nm(1187 nm–2253 nm) for considered layer thickness of D_H (153 nm) and D_B (242 nm), respectively.

The graded layer's boundary from the beginning to the end exhibits hyperbolic variations in the index of refraction, as represented in Equation (3) [24].

$$n_H\,(y) = \frac{n_i}{1 - \alpha y} \tag{2}$$

where α is the hyperbolic grading parameter evaluated as $[(n_f - n_i)/(n_f \cdot d_{defect})$, depicting the hyperbolic graded index layer with subscript H. The refractive indices at the beginning and end of the layer featuring a hyperbolic gradient can be denoted by n_i and n_f, respectively. Here, 'i' stands for the initial position and 'f' for the last point along the layers thickness. "d_{defect}" is the layer thickness.

Equation (4) provides the distribution of the field profile in a plane normal to the surface of the hyperbolic grading layer [24].

$$E_H(y) = A_H\sqrt{\xi_H} \cdot \cos(m \cdot \log(\xi_H)) + B_H\sqrt{\xi_H} \cdot \sin(m \cdot \log(\xi_H)) \tag{3}$$

where A_H and B_H are hyperbolic graded index layer constants. At normal incidence angle, the propagation wave vector is presented by the variable $\xi_H = 1 - \alpha x$, $m^2 = [(\omega n_i/c\alpha)^2 - (1/4)]$, and the velocity of light is represented by c, whereas ω denotes the radial frequency. The Transfer Matrix Method (TMM) is a suitable approach for assessing the reflection spectrum of multilayer 1D photonic crystals, particularly for analyzing both graded (hyperbolically variable) and non-graded structures of 1D multilayer resonators. The transfer matrix of a specific k^{th} layer is written as [25]

$$T_k = \begin{bmatrix} \cos\alpha_k & \frac{\sin\alpha_n}{q_n} \\ -iq_k \sin\alpha_k & \cos\alpha_k \end{bmatrix} \tag{4}$$

where $\alpha_k = \frac{2\pi}{\lambda_k n_k d_k \cos\theta_k}$ and $q_k = n_k \cos\theta_k$ for TE mode. n_k, d_k and θ_k are the index of refraction, width, and angle of propagation for the k^{th} layer, and λ_k is the resonating wavelength. 1550 nm is the resonating wavelength that is to be considered. The characteristic matrix for the proposed multilayer geometry can be obtained by multiplying each matrix for a single layer, as expressed in Equation (6).

$$T = \prod_{k=1}^{N} T_k = \begin{bmatrix} T_{11} & T_{12} \\ T_{21} & T_{22} \end{bmatrix} \tag{5}$$

The quantity N corresponds to the number of periods in the multilayer structure. The reflection coefficient of proposed multilayer geometry is given by Equation (7) [26].

$$r\,(\omega) = \frac{(T_{11} + T_{12}q_k)\,q_k - (T_{21} + T_{22}q_k)}{(T_{11} + T_{12}q_k) - (T_{21} + T_{22}q_k)} \tag{6}$$

Finally, the reflectance of the entire structure is calculated as $R = |r\,(\omega)|^2$.

3. RESULTS & DISCUSSIONS

In order to evaluate the reflection spectrum, bandgaps, quality factor, resonating wavelength, and field confinement profile of both non-graded resonator (NGR) and hyperbolic graded (HGR) based 1D photonic structures, the proposed multilayer structure has been numerically simulated using COMSOL 5.5. Initially, the multilayer periodic geometry with no defect layer was studied to assess the sensing capabilities of both non-graded NGR and graded HGR structures. Figure 2 shows the combined reflectance spectrum of non-graded and graded geometry at 0° angle of incidence. In the absence of a defect layer, a 100% reflection is achievable with $N = 8$ for the non-graded structure, where N refers to the number of periods required to achieve complete reflection within the desired bandgap. By assuming that the refractive index (n_{defect}) and width (d_{defect}) of the defect layer are n_A and D_A, respectively, the reflectance spectrum of a multilayer periodic geometry can be illustrated. It was observed that

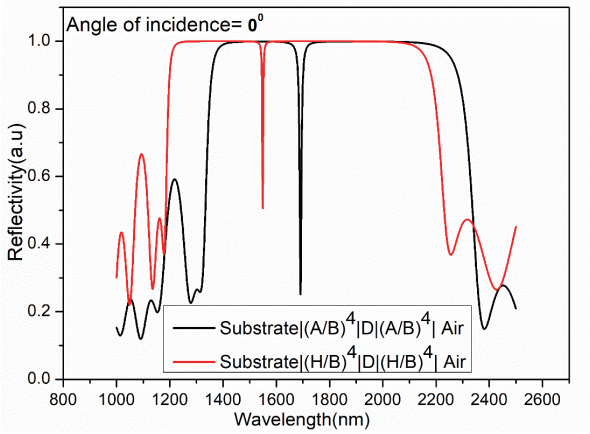

Figure 2. Combined reflectance spectrum of non-graded geometry (Substrate/$(AB)^4/D/(AB)^4$/air) with defect resonating at 1550 nm and graded geometry (Substrate/$(HB)^4/D/(HB)^4$/air) with defect resonating at 1691nm.

the structure resonates at 1550 nm and through optimization. It was found that the HGR structure exhibited 100% reflection within the 1066 nm band gap without a defect layer at $N = 8$ periods. A reflection dip at wavelength λ_{defect} results from the introduction of the cavity layer into the multilayer periodic geometry, which localizes the defect modes. The location of the resonating wavelength of 1691 nm in the HGR structure is established by the thickness of the sample and its refractive index as it passes through the defect layer.

3.1. Overview of Sensor Sensitivity, the Figure of Merit, and Detection Limit

The human body predominantly comprises triglycerides, high-density lipoproteins, and cholesterol as its lipid components. Because they are nonpolar and water-insoluble, triglycerides and cholesterol require transportation through the bloodstream with other lipoprotein particles. Triglycerides are a type of fat molecule found in the body and foods. They are composed of three fatty acids attached to a glycerol molecule. High levels of cholesterol pose greater health risks, increasing the likelihood of developing atherosclerosis, heart disease, and stroke. Hence, it is essential to monitor cholesterol levels regularly. Cholesterol can either benefit the cardiovascular system (through high-density lipoprotein) or impair it (through low-density lipoprotein). A desirable total blood cholesterol level is less than 200 mg/dl (5.17 mmol/L), while 200 to 239 mg/dl (5.17–6.18 mmol/L) is considered borderline high for heart disease, and 240 mg/dl (6.22 mmol/L) and higher is considered high blood cholesterol [27]. Table 1 [28] provides information on the refractive index of cholesterol levels. The Z-scan technique has been employed in experimental studies to obtain the refractive indices of samples with varying

Table 1. Refractive index of standard cholesterol level.

Standard Cholesterol Concentration (mg/dl)	Refractive index
200	2.49 ± 0.08
220	2.62 ± 0.09
240	2.80 ± 0.07
260	3.06 ± 0.06
280	3.23 ± 0.07
300	3.47 ± 0.09

concentrations of cholesterol. The dependence of refractive index (RI) on cholesterol concentration has been examined and confirmed.

As the concentration of cholesterol rises, there is a corresponding increase in refractive index, with steps of 20 mg/dl from normal (200 mg/dl) to high risk (300 mg/dl). The suggested sensor involves introducing a blood sample into a defect layer, causing a change in the depth of reflection from a standard cholesterol level of 200 mg/dl to different levels, including 220 mg/dl, 240 mg/dl, 260 mg/dl, 280 mg/dl, and 300 mg/dl.

The effective refractive index of the cavity layer changes when the analyte infiltrates it, leading to a shift in the resonance wavelength. This shift ($\Delta\lambda_r$) is used to determine the concentration of the analyte. The devices exhibit an average sensitivity ($S = \Delta\lambda_r/\Delta n$) [29, 30], where Δn is the refractive index variation in RIU. The proposed cavity structures are also evaluated based on their quality factor (Q) and figure of merit (FOM). The quality factor is determined by measuring the bandwidth between the half points of the maximum reflectance spectrum (FWHM) of the resonance peaks ($Q = \lambda_r/FWHM$) [31]. At the same time, the figure of merit is obtained as the ratio of sensitivity to FWHM ($FOM = S/FWHM$). In addition to sensitivity, Table 3 presents the computation and presentation of several other sensor parameters. The detection limit (DL) is the minimum variation in the refractive index that the sensor can detect. It is computed by dividing the sensor's resolution by its sensitivity, as described by equation [32]: ($DL= (SR/S)$). The minimum observable spectral shift is known as the sensor resolution (SR) and is calculated as ($SR = FWHM/1.5(SNR)^{0.25}$). The sensing performance of both structures is compared with respect to the width of the defect layer. The signal-to-noise ratio (SNR) is determined by ($SNR = \Delta\lambda_r/FWHM$) [33, 34]. The slope of the sensor's response sensitivity improves as the sample layer width and angle of incidence increase. The following subsection covers the impact of altering cavity width and changing incidence angle on the sensing performance of both non-graded and hyperbolically graded index photonic geometries.

3.2. Sensing Performance Assessment of the 1D Photonic Resonator Geometry (Both Non-Graded and Graded Index Structures)

Adding porosity to a layer in a periodic multilayer geometry facilitates the infiltration of analytes, thereby increasing the sensitivity of the sensor. This addition of porosity also leads to variation in the effective refractive index of each layer. Further research was conducted on the varying reflectivity of the cavity structure. The study involved injecting analytes containing different levels of cholesterol into the pores of the layer, which caused a shift in the resonating wavelength of the resonator in the reflectivity spectrum due to the alteration of the layer's effective refractive index. The initial design for the proposed structure involved a non-graded resonator consisting of alternate layers with refractive indices of 3.45 and 1.6. However, a grading in the high index layer has been introduced, which increases hyperbolically from 1.6 to 3.45. Using Equation (1), we found that the effective refractive index of the hyperbolically graded layer changed from 2.6814 to 3.4660. The refractive index of the lower index layer was taken to be 1.6.

The reflectance properties of a 1D photonic crystal with a cavity layer based on a proposed resonator with both non-graded and hyperbolically graded refractive indices have been examined. The study suggests that the sensor could be made highly sensitive by adjusting various factors, such as the angle of incidence, width of the defect layer, and cholesterol concentration. The sensitivities of non-graded and hyperbolically graded geometries have been compared at different angles of incidence (0-degree, 20-degree, and 40-degree) and by varying the width of the cavity layer from D_A to $2D_A$, as shown in Table 2. When the width of the cavity layer exceeds $2D_A$, unconfined modes are stimulated outside the desired bandgap. Figure 3 displays the reflectances of both the non-graded and graded index structures at an angle of incidence of 0 degrees with a defect layer thickness of D_A. Additional reflection spectra can be found in the supporting supplementary file, particularly in Figures S1, S2, and S3.

The sensitivity response of the proposed structure at varying cavity thicknesses is presented in Table 2. Increasing cavity layer width from D_A to $3D_A$ leads to the excitation of higher energy modes of improved sensitivity. The average sensitivity of a non-graded sensor with an angle of incidence 0 degrees and cavity width of D_A is 125 nm/RIU. In contrast, it is 268 nm/RIU for hyperbolically graded index structures. As a result, hyperbolically graded refractive index structures possess a sensitivity of nearly 114% increase compared to non-graded structures. Sensor back reflections are formed by a

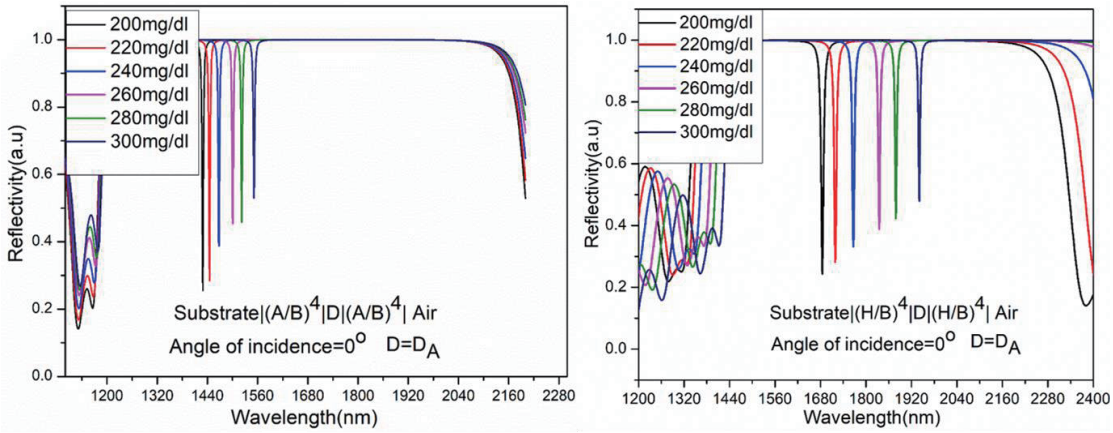

Figure 3. The influence of analyte infiltration on the cavity thickness $D = D_A$ is demonstrated for (a) the non-graded and (b) the hyperbolic graded geometry.

Table 2. Comparison of NGR and HGR structure's sensitivity at various cavity widths and incidence angles.

Cholesterol Concentration (mg/dl)	Incidence Angle	Non-Graded layer (NGR) Sensitivity (nm/RIU)			Graded layer (HGR) Sensitivity (nm/RIU)		
	θ	$D=D_A$	$D=1.5D_A$	$D=2D_A$	$D=D_A$	$D=1.5D_A$	$D=2D_A$
220	0°	123	169	232	276	330	453
240		125	174	216	274	335	409
260		128	177	208	264	336	401
280		125	177	208	267	336	394
300		125	174	197	260	329	384
220	20°	138	207	246	276	361	423
240		141	196	235	283	364	416
260		138	196	226	273	352	403
280		136	189	217	294	348	397
300		135	183	210	271	350	391
220	40°	184	269	292	323	379	469
240		174	254	274	329	387	445
260		173	236	261	312	389	428
280		174	227	250	308	381	425
300		168	218	238	305	377	420

further rise in incidence angle. Figure 4(a) displays a chart comparing the sensitivity of non-graded and graded index structures for varying incident angles and a cavity layer width of D_A. Average sensitivity summary of both the geometry with respect to cavity thickness is represented in a linear graph in Figure 4(b). The HGR sensor of width $2D_A$ shows a maximum sensitivity of 437 nm/RIU, the detection limit of 7.5×10^{-3}, and figure of merit (FOM) of 234.5 RIU^{-1} shown in Table 3.

Figure 5(a) displays a reflection spectrum from the HGR structure (Substrate/$(HB)^4/D/(HB)^4$/air) at a defect layer thickness of $2D_A$ and a 40-degree angle of incidence. The structure also possesses a very high electric field intensity about 3.7×10^5 v/m, 2.6×10^{-3} v/m, and 2.3×10^{-3} v/m for 0-degree,

Table 3. For various cholesterol concentrations, sensor resolution, the figure of merit, sensitivity, detection limit, and signal-to-noise ratio of the hyperbolic graded refractive index sensor at an incidence angle of 40° and a d_{defect} of $2D_A$ are presented.

Cholesterol Concentration (mg/dl)	Sensor resolution	FOM (RIU^{-1})	Sensitivity (nm/RIU)	Detection limit	Signal-to-Noise Ratio
220	3.539417	234.5	469	0.007547	31
240	3.641916	111.25	445	0.008184	34.75
260	4.509231	142.6667	428	0.010536	81.6666667
280	4.222612	85	425	0.009936	62.8
300	4.010972	52.5	420	0.00955	51.125

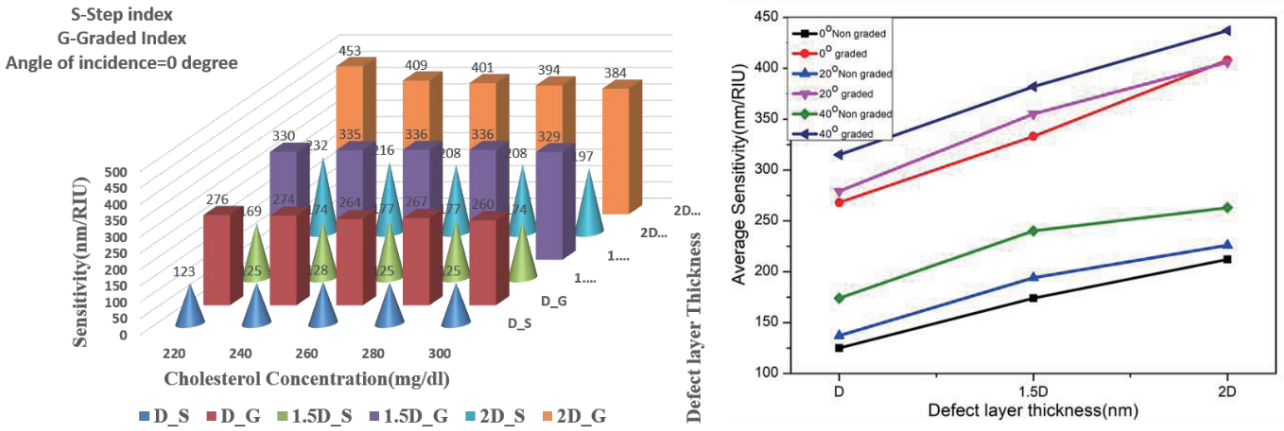

(a) (b)

Figure 4. (a) The sensitivity of the non-Graded layer (NGR) and Graded layer (HGR) structures is compared at different angles of incidence and various defect layer thicknesses. (b) Average Sensitivity summary of both the geometry with respect to cavity thickness.

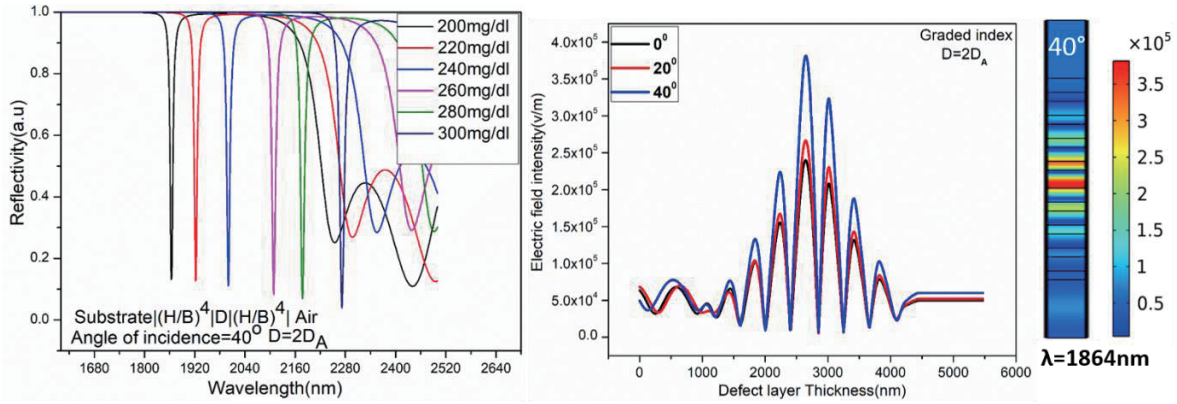

(a) (b)

Figure 5. (a) shows the reflection spectrum of a Graded layer (HGR) structure (Substrate/$(HB)^4/D/(HB)^4$/air) at $D = 2D_A$ and a 40-degree angle of incidence. (b) The electric field distribution at the surface of a graded index structure at $D = 2D_A$ with various incidence angle.

20-degree, and 40-degree incidence angles shown in Figure 5(b).

In conclusion, changing the incidence angle can improve the sensitivity of the proposed bio-photonic sensor for a given cavity layer thickness, leading to improved performance. The use of a graded index profile results in improved sensitivity compared to a conventional non-graded profile by reducing interface-assisted losses in the multilayer geometry. The introduction of a hyperbolically graded index strongly influences the mode confinement property of the geometry, resulting in confined mode electric field intensity in the cavity region (3.7×10^5 V/m) and enhancing light-matter interaction. In terms of detecting cholesterol at various concentrations, the recommended structure outperforms others in terms of sensing performance. The sensitivity of the exponentially graded structure has been determined in our previous work [35] as 438.70 nm/RIU. However, in the present work, the sensitivity of the hyperbolically graded structure was found to be 469 nm/RIU. Also, there is an improvement in surface electric field confinement in hyperbolically graded geometry compared to the exponentially graded geometry. The subsequent section discusses important applications and previously reported designs.

Table 4 is presented to facilitate a comparison of the results obtained in this study with those from earlier research in the photonic field. This comparison is based upon a refractive index sensing mechanism that focuses on the sensitivity of the proposed graded 1D photonic structure with the previously reported designs. By changing the incidence angles, the proposed structure's sensitivity may be simply increased without having to meet any phase-matching constraints, unlike structures based on surface plasmon resonance (SPR). The use of current thin film deposition processes makes it simpler to fabricate the suggested design. Table 4 clarifies that compared to current bio-sensing research efforts, the proposed biosensor has substantially higher performance and a comparatively strong sensitivity for detecting cholesterol levels.

Table 4. Comparative performance analysis with recently reported results.

Reference	Sensitivity (nm/RIU)	Detection limit	Year
[36]	290	-	2021
[37]	100	10^{-5}	2021
[38]	214.28	-	2023
[39]	387.5	2.44×10^{-4}	2021
...	469	7.5×10^{-3}	Our proposed work

4. CONCLUSION

This study presents an innovative photonic crystal cavity structure that incorporates a graded refractive index, enabling precise control and modification of light propagation. The structure is composed of a porous bilayer 1D-PC structure, comprising silicon and porous silicon, where the refractive index of the high index layer is modulated hyperbolically across its width and is arranged as $[(HB)^4/D/(HB)^4]$. The introduction of porosity allows for a significant contrast in refractive index within the same material, resulting in minimal losses due to interfaces. Moreover, it facilitates convenient adjustment of mode dispersion properties and scalability in design for any desired wavelength range as specified by the user. This structure is used to detect cholesterol content and has a sensitivity that is 114% better than the equivalent non-graded structure. The graded index structure allows for the tuning of various factors, including incidence angle and cavity width, to adjust the photonic band gap width, reflection mode intensity, and position. A graded layer can be physically implemented because the porous material enables analytes to infiltrate easily. The hyperbolically graded design demonstrates exceptional sensitivity of 469 nm/RIU and a detection limit of 7.5×10^{-3} when blood samples containing cholesterol concentrations of 240 mg/dl are introduced at room temperature into a defect layer with a thickness of $2D_A$. The proposed sensor's benefits, such as compact size, low manufacturing cost, improved sensitivity, and suitability for mass production, make it a promising candidate for biomedical applications.

REFERENCES

1. Robertson, W. M., "Experimental measurement of the effect of termination on surface electromagnetic waves in one-dimensional photonic bandgap arrays," *Journal of Lightwave Technology*, Vol. 17, No. 11, 2103–2017, 1999, doi: 10.1109/50.802988.
2. Goyal, A. K., and J. Saini, "Performance analysis of Bloch surface wave based sensor using transition metal dichalcogenides," *Applied Nanoscience*, Vol. 10, No. 11, 4307–4313, 2020.
3. Goyal, A. K. and Y. Massoud, "Interface edge mode confinement in dielectric-based quasi-periodic photonic crystal structure," *Photonics*, Vol. 9, No. 676, 2022, https://doi.org/10.3390/photonics9100676.
4. Goyal, A. K., M. Hussain, and Y. Massoud, "Analysis of interface mode localization in disordered photonic crystal structure," *J. Nanophoton.*, Vol. 16, No. 4, 046007, 2022, DOI: 10.1117/1.JNP.16.046007.
5. Goyal, A. K., and S. Pal, "Design and simulation of high-sensitive gas sensor using a ring-shaped photonic crystal waveguide," *Phys. Scr.*, Vol. 90, 2015, https://doi.org/10.1088/0031-8949/90/2/025503.
6. Goyal, A. K., "Design analysis of one-dimensional photonic crystal based structure for hemoglobin concentration measurement," *Progress In Electromagnetics Research M*, Vol. 97, 2020, https://doi.org/10.2528/pierm20080601.
7. Kurt, H. and D. S. Citrin, "Graded index photonic crystals," *Optics Express*, Vol. 15, No. 3, 1240, 2007, https://doi.org/10.1364/OE.15.001240.
8. Zhu, Q., L. Jin, and Y. Fu, "Graded index photonic crystals: A review," *Ann. Phys.*, Vol. 527, 205–218, 2015.
9. Singh, B. K., M. K. Chaudhari, and P. C. Pandey, "Photonic and omnidirectional band gap engineering in one-dimensional photonic crystals consisting of linearly graded index material" *Journal of Lightwave Technology*, Vol. 34, 2431–2438, 2016, https://doi.org/10.1109/JLT.2016.2531900.
10. Russel, P. S. J. and T. A. Birks, "Hamiltonian optics of nonuniform photonic crystals," *Journal of Lightwave Technology*, Vol. 17, 1982–1988, 1999.
11. Centeno, E. and D. Cassagne, "Graded photonic crystals," *Opt. Lett.*, Vol. 30, 2278–2280, 2005, https://doi.org/10.1364/OL.30.002278.
12. Centeno, E., D. Cassagne, and J. P. Albert "Mirage and superbending effect in two dimensional graded photonic crystals," *Phys. Rev. B*, Vol. 73, No. 23, 235119, 2006, https://doi.org/10.1103/PhysRevB.73.235119.
13. Singh, B. K., A. Bijalwan, and P. C. Pandey, "Rastogi V (2020) Multi-channel photonic bandgap consequences in one-dimensional linear, exponential, and hyperbolic graded-index photonic crystals," *Journal of the Optical Society of America B*, Vol. 37, 523, https://doi.org/10.1364/josab.381681.
14. Belhadj, W. and A. N. Al-Ahmadi, "Tunable narrowband terahertz multichannel filter based on one-dimensional graphene-dielectric photonic crystal," *Optical and Quantum Electronics*, Vol. 53, 2021, https://doi.org/10.1007/s11082-020-02642-9.
15. Alagappan, M., S. Immanuel, R. Sivasubramanian, and A. Kandaswamy, "Development of cholesterol biosensor using Au nanoparticles decorated f-MWCNT covered with polypyrrole network," *Arabian Journal of Chemistry*, Vol. 13, 2001–2010, 2020, https://doi.org/10.1016/j.arabjc.2018.02.018.
16. Nguyen, P. T., Y. I. Kim, and M. I. Kim, "Reagent-free colorimetric cholesterol test strip based on self color-changing property of nanoceria," *Frontiers in Chemistry*, Vol. 8, 2020, https://doi.org/10.3389/fchem.2020.00798.
17. Yantih, N., W. Destiana, and D. K. Pratami, "Anti-choloseterol activities of white (Raphanus raphanistrum) and red (raphanus sativus) radish roots," *International Journal of Applied Pharmaceutics*, Vol. 13, No. 2, 2021, https://doi.org/10.22159/ijap.2021.v13s2.05.

18. Kolarič, L. and P. Šimko, "The comparison of hplc and spectrophotometric method for cholesterol determination," *Potravinarstvo Slovak Journal of Food Sciences*, Vol. 14, 2020, https://doi.org/10.5219/1302.
19. Ghosh, G., *Handbook of Thermo-Optic Coefficients of Optical Materials with Applications*, 1997.
20. Dash, D., J. Saini, A. K. Goyal, and Y. Massoud, "Exponentially index modulated nanophotonic resonator for high-performance sensing applications," *Scientific Report*, Vol. 13, 1431, 2023, https://doi.org/10.1038/s41598-023-28235-6.
21. Wiederseiner, S., N. Andreini, G. Epely-Chauvin, and C. Ancey, "Ancey Refractive-index and density matching in concentrated particle suspensions: A review," *Exp. Fluids*, Vol. 50, 1183–1206, 2011, https://doi.org/10.1007/s00348-010-0996-8.
22. Goyal, A. K., A. Kumar, and Y. Massoud, "Performance analysis of DAST material-assisted photonic-crystal-based electrical tunable optical filter," *Crystals*, Vol. 12, No. 7, 992, 2022.
23. Ratra, K., M. Singh, and A. K. Goyal, "Design and Analysis of Omni-directional Solar Spectrum Reflector using One-dimensional Photonic Crystal," *J. Nanophoton.*, Vol. 14, No. 2, 026005, 2020.
24. Singh, B. K., V. Bambole, V. Rastogi, and P. C. Pandey, "Multi-channel photonic bandgap engineering in hyperbolic graded index materials embedded one-dimensional photonic crystals," *Opt. Laser Technol.*, Vol. 129, 2020, doi: 10.1016/j.optlastec.2020.106293.
25. Yeh, P. and M. Hendry, "Optical waves in layered media," *Physics Today*, Vol. 43, 1990, https://doi.org/10.1063/1.2810419.
26. Sharma, S., R. Kumar, K. S. Singh, A. Kumar, and V. Kumar, "Omnidirectional reflector using linearly graded refractive index profile of 1D binary and ternary photonic crystal," *Optik (Stuttg)*, Vol. 126, No. 11–12, 1146–1149, 2015, doi: 10.1016/j.ijleo.2015.03.029.
27. Ma, H., *Cholesterol and Human Health. Nature and Science*, Vol. 2, No. 4, (Supplement): 17–21, 2004.
28. Dhinaa, A. N. and P. K. Palanisamy, "Z-scan technique for measurement of total cholesterol and triglycerides in blood," *Journal of Innovative Optical Health Sciences*, Vol. 02, No. 03, 295–3012, 2009, https://doi.org/10.1142/S1793545809000565.
29. Pathania, P. and M. S. Shishodia, "Fano resonance-based blood plasma monitoring and sensing using plasmonic nanomatryoshka," *Plasmonics*, Vol. 16, No. 6, 2117–2124, 2021, doi: 10.1007/s11468-020-01343-z.
30. Goyal, A. K., H. S. Dutta, and S. Pal, "Development of uniform porous one-dimensional photonic crystal based sensor," *Optik*, Vol. 223, 165597, 2020.
31. Meng, Q. Q., X. Zhao, C. Y. Lin, S. J. Chen, Y. C. Ding, and Z. Y. Chen, "Figure of merit enhancement of a surface plasmon resonance sensor using a low-refractive-index porous silica film," *Sensors*, Vol. 17, No. 8, Switzerland, 2017, doi: 10.3390/s17081846.
32. Edappadikkunnummal, S., R. V. Chembra, S. Dinesh, et al., "Detection of hemoglobin concentration based on defective one-dimensional photonic crystals," *Photonics*, Vol. 9, 2022, https://doi.org/10.3390/photonics9090660.
33. Gowda, R. B., P. Sharan, and K. Saara, "1-Dimensional silicon photonic crystal pressure sensor for the measurement of low pressure," *Results in Optics*, Vol. 10, 2023, doi:10.1016/j.rio.2023.100352.
34. Goyal, A. K., H. S. Dutta, and S. Pal, "Performance optimization of photonic crystal resonator based sensor," *Optical and Quantum Electronics*, Vol. 48, 431, 2016.
35. Dash, D. and J. Saini, "Sensitivity analysis of non-graded and graded index one dimensional cavity-based cholesterol sensor," *Optical and Quantum Electronics*, Vol. 55, 349, 2023, https://doi.org/10.1007/s11082-023-04587-1.
36. Panda, A., P. D. Pukhrambam, F. Wu, and W. Belhadj, "Graphene-based 1D defective photonic crystal biosensor for real-time detection of cancer cells," *European Physical Journal Plus*, Vol. 136, 2021, https://doi.org/10.1140/epjp/s13360-021-01796-z.
37. Aly, A. H., S. K. Awasthi, D. Mohamed, et al., "Study on a one-dimensional defective photonic crystal suitable for organic compound sensing applications," *RSC Advances*, Vol. 11, 32973–32980, 2021, https://doi.org/10.1039/d1ra06513k.

38. Panda, A. and P. D. Pukhrambam, "Study of metal-porous GaN-based 1D photonic crystal tamm plasmon sensor for detection of fat concentrations in milk," *Micro and Nanoelectronics Devices, Circuits and Systems*, Vol. 904, 415–425,2023, https://doi.org/10.1007/978-981-19-2308-1_42.
39. Panda, A. and P. D. Pukhrambam, "Investigation of defect based 1D photonic crystal structure for real-time detection of waterborne bacteria," *Physica B: Condensed Matter*, Vol. 607, 2021, https://doi.org/10.1016/j.physb.2021.412854.